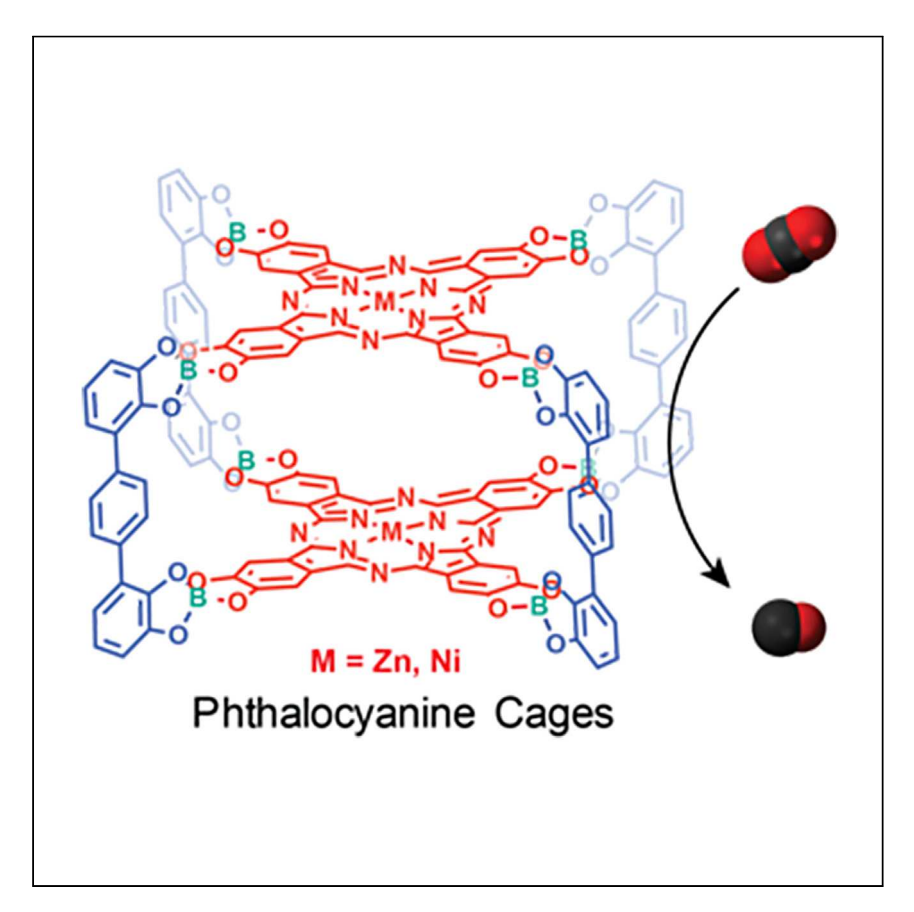


### Report

## Shape-persistent phthalocyanine cages



Hu et al. report the one-step synthesis of phthalocyanine-based molecular cages via dynamic spiroborate exchange. Owing to the site-isolated metal centers, readily accessible intrinsic cavity, and shape-persistent backbone, the nickel-metallated cage exhibits notable electrocatalytic  ${\rm CO_2RR}$  performance, demonstrating the feasibility of incorporating catalytically active moieties into cage structures to achieve enhanced catalytic activity.

Yiming Hu, Shaoda Huang, Lacey J. Wayment, ..., Mingliang Du, Shuanglong Lu, Wei Zhang

lushuanglong@jiangnan.edu.cn (S.L.) wei.zhang@colorado.edu (W.Z.)

#### Highlights

Well-defined phthalocyaninebased molecular cages are synthesized in high yields

The one-step cage synthesis is accomplished via dynamic spiroborate exchange

The cage structure is elucidated by single-crystal X-ray diffraction

Ni-metallated cage shows high selectivity in electrocatalytic CO<sub>2</sub>RR in broad voltages

Hu et al., Cell Reports Physical Science 4, 101285

February 15, 2023 © 2023 The Author(s). https://doi.org/10.1016/j.xcrp.2023.101285





#### Report

## Shape-persistent phthalocyanine cages

Yiming Hu,<sup>1,6</sup> Shaoda Huang,<sup>2,6</sup> Lacey J. Wayment,<sup>1</sup> Jingyi Wu,<sup>1</sup> Qiucheng Xu,<sup>1</sup> Tieyan Chang,<sup>3</sup> Ying-Pin Chen,<sup>3</sup> Xiaonian Li,<sup>4</sup> Babak Andi,<sup>5</sup> Hongxuan Chen,<sup>1</sup> Yinghua Jin,<sup>1</sup> Han Zhu,<sup>2</sup> Mingliang Du,<sup>2</sup> Shuanglong Lu,<sup>2,\*</sup> and Wei Zhang<sup>1,7,\*</sup>

#### **SUMMARY**

Phthalocyanine (Pc), an electro-redox active moiety, has many attractive properties stemming from its large aromatic system and ability to act as a catalyst in electrochemical reactions, such as the CO<sub>2</sub> reduction reaction (CO<sub>2</sub>RR). However, due to the synthetic challenge related to geometric requirements and poor solubility (strong aggregation), discrete shape-persistent cages consisting of site-isolated, readily accessible Pc moieties have not been available. Here, we report the synthesis of Zn- and Ni-metallated Pc-based molecular cages via one-step dynamic spiroborate linkage formation in high yields. The ZnPc cage structure is unambiguously elucidated at the atomic level by single-crystal X-ray diffraction. Moreover, owing to the site-isolated redox-active metal centers, readily accessible intrinsic cavity, and shape-persistent backbone, the Ni-metallated Pc (NiPc) cage exhibits high catalytic efficiency, selectivity, and stability, superior to the non-caged control molecules in electrocatalytic CO<sub>2</sub>RR.

#### INTRODUCTION

Organic molecular cages (OMCs), also known as covalent organic polyhedrons (COPs), are an intriguing class of molecules with internal void space that have garnered considerable research interest over the past few decades. By employing dynamic covalent chemistry, a large variety of OMCs have been synthesized methodically with customized functionalities and cavity sizes.<sup>2–7</sup> Their unique cavity has been utilized in various applications, such as host-guest recognition, 5,6,8,9 gas adsorption, 1,4 controlled nano-particle growth, 10-13 and catalysis. 14-16 However, the design and synthesis of OMCs, particularly those with functional moieties and large cavity size (nm scale), still represent a challenging task due to the limited types of dynamic covalent linkages and functional building blocks. For example, OMCs consisting of functional panels such as porphyrins<sup>5,8,17</sup> and phthalocyanines with electrocatalytic activities are scarce. When shape-persistent functional panels are used as the building blocks, OMCs with a well-defined and non-collapsible cavity surrounded by multiple isolated catalytically active sites can be obtained, which can serve as reaction vessels with efficient mass transfer. For example, Kim and coworkers reported rigid molecular boxes consisting of multiple porphyrin panels,<sup>2</sup> which could significantly enhance the exposure of the porphyrin reactive centers and enable efficient electrocatalysis 18,19 and ion conduction. 20

Phthalocyanines (Pcs) are synthetic analogs of porphyrins that have intriguing redoxactive behaviors, metal-coordination abilities, light harvesting, and excellent thermal and chemical stabilities. Pcs have shown many attractive properties as electro-redox active moieties in electrochemical reactions, including the oxygen

lushuanglong@jiangnan.edu.cn (S.L.), wei.zhang@colorado.edu (W.Z.) https://doi.org/10.1016/j.xcrp.2023.101285



<sup>&</sup>lt;sup>1</sup>Department of Chemistry, University of Colorado Boulder, Boulder, CO, USA

<sup>&</sup>lt;sup>2</sup>Key Laboratory of Synthetic and Biological Colloids, Ministry of Education, School of Chemical and Material Engineering, Jiangnan University, Wuxi, Jiangsu, China

<sup>&</sup>lt;sup>3</sup>NSF's ChemMatCARS, The University of Chicago, Lemont, IL, USA

<sup>&</sup>lt;sup>4</sup>State Key Laboratory of Phytochemistry and Plant Resources in West China, Kunming Institute of Botany, Chinese Academy of Sciences, and Yunnan Key Laboratory of Natural Medicinal Chemistry, Kunming, Yunnan, China

<sup>&</sup>lt;sup>5</sup>Center for BioMolecular Structure, NSLS-II, Brookhaven National Laboratory, Upton, NY, USA

<sup>&</sup>lt;sup>6</sup>These authors contributed equally

<sup>&</sup>lt;sup>7</sup>Lead contact

<sup>\*</sup>Correspondence:



reduction reaction (ORR), hydrogen evolution reaction (HER), and CO<sub>2</sub> reduction reaction (CO<sub>2</sub>RR). <sup>21-26</sup> However, because of their planar structures and strong  $\pi$ - $\pi$ interactions between the Pc molecules, 27 Pcs tend to aggregate and are much less soluble, which causes difficulty in processing and also limits the accessibility of active sites. It was envisioned that when Pcs are integrated in the rigid backbone of OMCs, maximum exposure of these catalytically active sites and reaction efficiency could be achieved with the assistance of the internal cavity surrounded by multiple entry and exit windows for reactants and products. However, synthesis of Pc-based OMCs is far more challenging due to the presence of excessive reactive substituents, stringent vertex angle requirements, and the low solubility of rigid Pc panels. Unlike porphyrins, which are generally substituted with tetra-symmetric functional groups, the common structures of Pcs have octa- or hexadeca-symmetric substituents, which significantly increases the difficulty and complexity of connecting them to make a closed structure. Ball-type Pc cages consisting of two Pc molecules with four side arms have been reported.<sup>28</sup> However, only a mixture of stereoisomers was obtained in an extremely low yield (<5%-6%). To the best of our knowledge, discrete Pc cages with atomically precise structures have not been reported.

Herein, we report the first synthesis of well-defined Pc-based OMCs (Zn-metallated Pc [ZnPc] and Ni-metallated Pc [NiPc] cages) via one-step dynamic spiroborate formation in high yields (~70%). The shape-persistent structure of ZnPc was determined at the atomic level by single-crystal X-ray diffraction analysis. The synthesis was accomplished by exploiting the dynamic nature of spiroborate linkages formed from two diol moieties and boric acid. The thermodynamically favored [4 + 2] cages were obtained preferentially from the linear ditopic diol (1,1':4',1"-terphenyl]-2,2",3,3"-tetrol [Tp-4OH]) and tetratopic Pc diol (octahydroxyl-metallophthalocyanine [MPc-8OH]) through a self-sorting process. The single-component spiroborate-linked macrocycles were not observed. Given the site-isolated redox-active metal centers, readily accessible cavity, and shape-persistent backbone, the NiPc cage showed exceptionally high efficiency, selectivity, and stability in the electrocatalytic  $CO_2RR$  in a wide voltage range (0.8–2.0 V (vs. reversible hydrogen electrode [RHE])). It almost exclusively generates CO with a selectivity of 98.7% at -1.2 V (vs. RHE). More importantly, the selectivity was maintained at over 95% in the long-term durability tests. NiPc cage shows 13-fold higher turnover frequencies (TOFs) and much higher CO/H<sub>2</sub> selectivity compared with the non-caged control molecules, suggesting the advantages of integrating electrocatalytically active NiPc moieties into a molecular cage structure.

#### **RESULTS AND DISCUSSION**

#### Design and synthesis of Pc cages

The synthesis of Pc-based OMCs was accomplished by exploiting the dynamic nature of spiroborate linkages formed from diol-boric acid condensation. Pc derivatives generally have a planar structure with eight reactive sites. We envisioned the formation of Pc-based OMCs can be significantly simplified if octa-topic Pc moieties can be converted into tetra-topic building units, which have been widely used in the formation of a molecular cage. Reversible spiroborate formation <sup>29–31</sup> was thus chosen as the dynamic reaction because (1) they can be easily formed through the reaction between two diols and boric acid. Therefore, octa-topic Pc moieties can be simplified to tetra-topic building units, requiring only four linkers, similar to the porphyrin case. (2) Spiroborate linkages have a tetrahedral geometry with an angle between the two diol moieties close to 90°, providing the perfect angle for a cubic-shaped cage molecule. (3) The spiroborate formation is reversible and thus can

#### Report



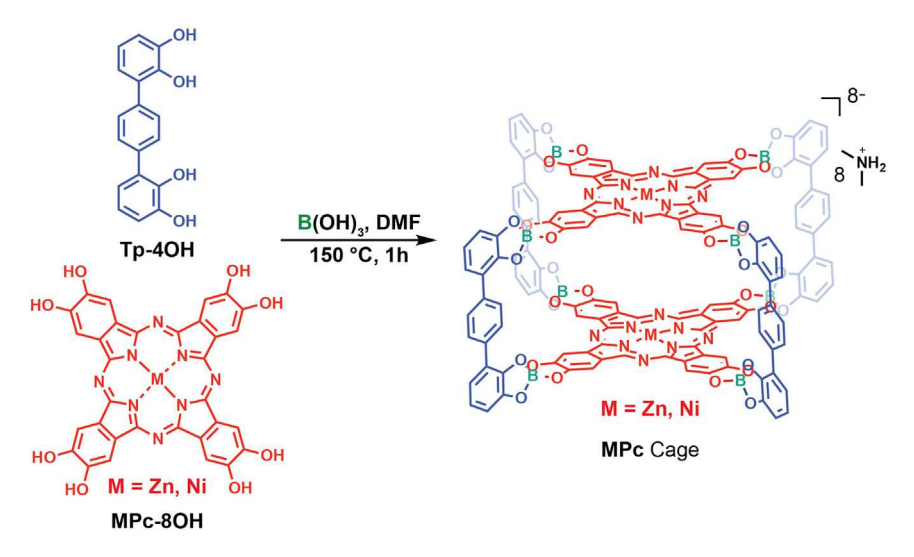


**Figure 1. Phthalocyanine cages**The synthesis of the ZnPc and NiPc cages.

provide a thermodynamically most stable species at the equilibrium through an error-correction mechanism. To our delight, the thermodynamically favored cubic-shaped [4 + 2] Pc cages could be successfully obtained from a tetratopic Pc diol, MPc-8OH; a linear ditopic diol, Tp-4OH; and boric acid (Figure 1). By incorporating different metal ions into Pcs, we obtained ZnPc and NiPc molecular cages in a modular fashion. Due to the poor solubility of MPc-8OH and the strong polarity of the cage product containing eight spiroborate anions, the solvent selection was limited to polar solvents, such as DMF, and DMSO, DMAc, or NMP. The formation of discrete cage molecules is entropically favored compared with the formation of polymers. Therefore, an elevated temperature can not only enhance the solubility of the intermediates but also promote the formation of the cage product. We found that heating the mixture of Tp-4OH and MPc-8OH in DMF at 150°C for 1 h can provide the cage product in around 70% yield.

It should be noted that the covalent assembly of OMCs has typically utilized asymmetric dynamic linkages with directionality, such as hydrogen bonds, metal-ligand dative interactions, and imine bonds. Such directionality requires two complementary functional groups and prevents self-reaction of monomers, therefore providing additional control over the assembly process. However, spiroborate linkages are symmetrical without directionality (i.e., two same diols react with one boric acid), allowing reactions between different diols as well as self-reaction of the same diols, which undoubtedly increases the complexity of the dynamic system. For example, when there are two different diol groups, they can form single-component or mixed multi-component species. Therefore, the geometry of building blocks and functional group orientation is critical to promoting the self-sorting process and formation of the thermodynamically most stable species. In the present case, although three molecules of Tp-4OH can react with three molecules of boric acid to form a cyclic trimer, the dynamic system provided ZnPc or NiPc cages as the predominant species at the equilibrium through the thermodynamically driven self-sorting process.

#### X-ray crystallographic analysis

Both the ZnPc and NiPc cages were soluble in DMF and DMSO and purified by recrystallization. They were characterized using nuclear magnetic resonance



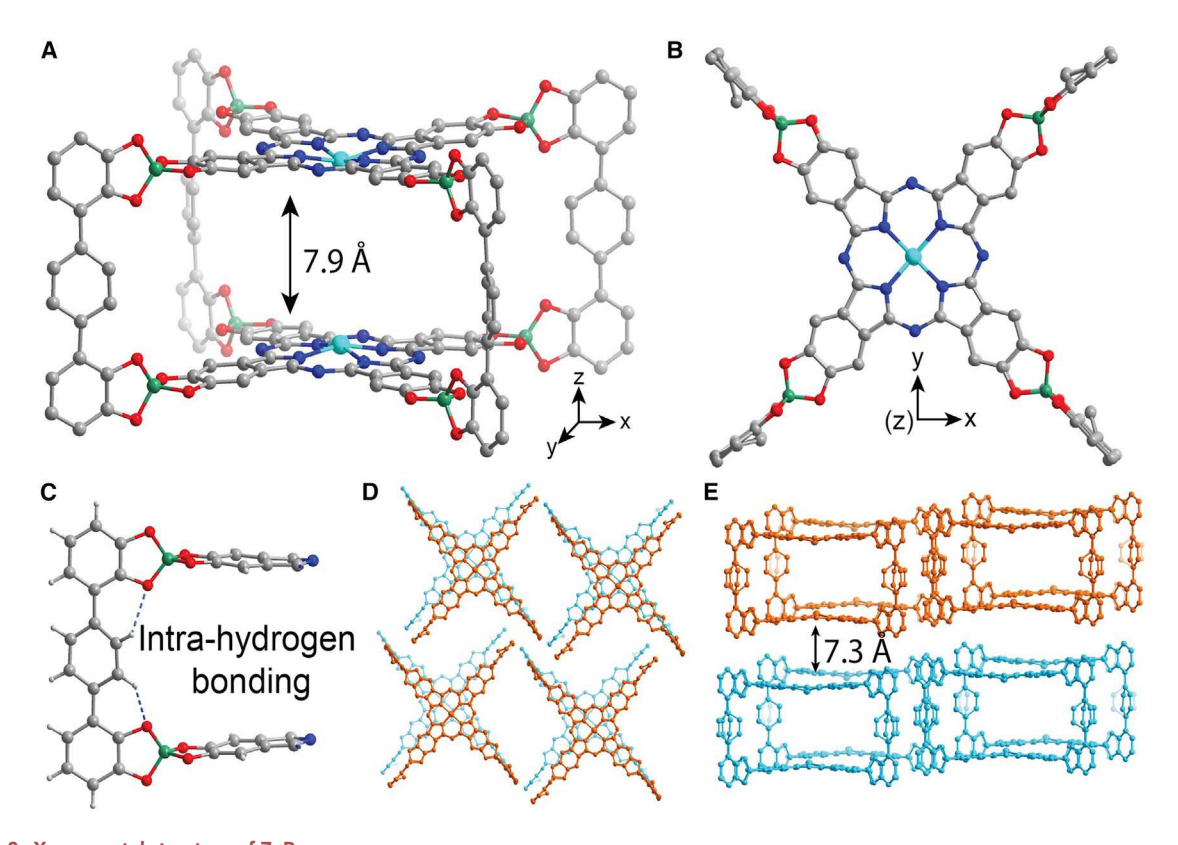


Figure 2. X-ray crystal structure of ZnPc cage
(A and B) Side view (A) and top view (B) of the ZnPc cage (C: gray, N: navy, O: red, B: green, Zn: blue).
(C–E) The intrahydrogen bonding between side arm and formed borate linkage (C). The packing structure of the ZnPc cage viewed from top (D) and side
(E). Hydrogen atoms, disordered solvent molecules, and disordered dimethyl ammonium were omitted for clarity.

(NMR) spectroscopy, gel permeation chromatography, electrospray ionization mass spectrometry (ESI-MS) analysis, and single-crystal X-ray analysis (Figures S1-S16 and Table S1). The dark green crystals of the ZnPc cage were grown by slow diffusion of ethanol to a saturated DMF solution for 1 week. The structure of the ZnPc cage was unambiguously determined by synchrotron X-ray diffraction with a discrepancy factor R of 9.88%, which unveils the structural information of the cage and its packing pattern (Figure 2). The triclinic unit cell (a = 15.004 Å, b = 20.234 Å, c = 20.979 Å, and  $\alpha = 93.894^{\circ}$ ,  $\beta = 97.289^{\circ}$ , and  $\gamma = 93.217^{\circ}$ , space group  $\overline{P1}$ ) was found containing a single cage molecule. Due to the insufficient diffractions, the precise location of dimethylammonium counterions and disordered solvents were difficult to determine. The crystal structure shows that two Pc panels and four side arms are connected perpendicularly through eight spiroborate linkages, forming a cubic-shaped cage with an internal distance of 7.5 Å between the two Pc centers. The top Pc panel is almost perfectly overlaid with the bottom one, showing the high rigidity of the cage with little distortion. Surprisingly, we found that the middle benzene ring of Tp-4OH moieties is eclipsed by the adjacent benzene rings, which is rare given that the majority of the p-terphenyl groups have staggered conformation for the central benzene ring to achieve lower energy. This is likely due to the intramolecular hydrogen bonding interactions between the oxygen atoms in spiroborate linkage and the proton of the middle benzene ring (dO●●●H = 2.5 Å; Figure 2C). However, the protons of the middle benzene ring are magnetically equivalent in the <sup>1</sup>H NMR spectrum, indicating that the middle benzene ring is free to rotate in solution at



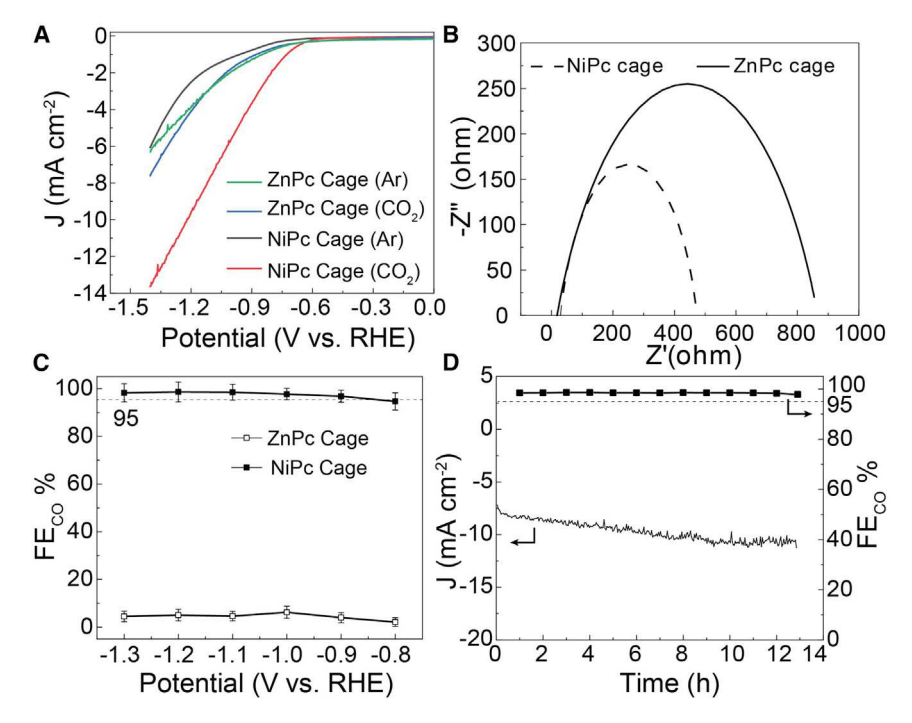


Figure 3. CO<sub>2</sub> electrochemical reduction by ZnPc and NiPc cages

- (A) LSV curve of ZnPc and NiPc cages under Ar- and  $CO_2$ -saturated 0.1 M KHCO $_3$  solution, respectively.
- (B) The fitted Nyquist plots of NiPc and ZnPc cages.
- (C) CO faradaic efficiency of ZnPc and NiPc cages.
- (D) Stability test of NiPc cage at -1.2 V for 13 h.

The error bars represent the standard deviation from at least three independent measurements.

room temperature. The cages stack along the z axis with an offset of approximately  $1.5\ \text{Å}.$ 

#### CO<sub>2</sub> electrochemical reduction

The shape persistency of Pc molecular cages renders non-collapsible, well-defined intrinsic cavities and isolated, readily accessible catalytically active sites, which make them highly attractive for the electrocatalytic CO<sub>2</sub>RR. In addition, the ability of Pcs binding different metal ions provides the great tunability of their redox-active properties. We demonstrate the significant difference in CO<sub>2</sub>RR performance of NiPc and ZnPc Pc cages. The electrochemical properties of ZnPc and NiPc were evaluated using a standard two-compartment electrochemical cell in CO<sub>2</sub>-saturated 0.1 M KHCO<sub>3</sub> electrolyte. All measured electrode potentials were converted to RHE. The linear sweep voltammetry (LSV) tests were performed in Ar- and CO<sub>2</sub>-saturated electrolytes in the potential range from 0 to -1.4 V at a scan rate of 5 mV s<sup>-1</sup> (Figure 3A). The LSV curve of the NiPc cage in CO<sub>2</sub>-saturated solution shows a significantly larger current density and a substantially smaller onset potential than those in Ar-saturated solution, indicating the strong interactions between the NiPc cage and CO<sub>2</sub> molecules. By contrast, the LSV results show that the ZnPc cage exhibits similar current density and onset potential in CO<sub>2</sub>- and Ar-saturated electrolytes, indicating that there are no strong interactions between the ZnPc cage and CO<sub>2</sub>. In addition, the onset potential of the NiPc cage was -0.60 V in CO<sub>2</sub>-saturated solution, which is higher than that of the ZnPc cage (-0.74 V). The electrochemical double-layer capacitance (C<sub>dl</sub>) was applied to determine the electrochemically active surface area (ECSA) (Figure S17). Interestingly, the NiPc cage also has a higher C<sub>dl</sub> value





of 3.55 mF cm $^{-2}$  than the ZnPc cage (2.27 mF cm $^{-2}$ ). These results suggest that the NiPc cage likely has superior CO $_2$ RR activity to the ZnPc cage. To further explore the electrocatalytic kinetics on the electrode/electrolyte surface, the electrochemical impedance spectroscopy (EIS) (Figure 3B) and Tafel slope were analyzed (Figure S18). The NiPc cage has a substantially lower charge-transfer resistance and Tafel slope value compared with the ZnPc cage, indicating that the NiPc cage is kinetically preferred during the CO $_2$ RR process.

To determine the selectivity of as-prepared catalysts, we analyzed the reduction products using gas chromatography (GC) and <sup>1</sup>H NMR spectroscopy. The result indicates that CO and H2 were the dominant products with no liquid product observed. Accordingly, the faradaic efficiency for CO (FE<sub>CO</sub>) and H<sub>2</sub> (FE<sub>H2</sub>) was calculated to evaluate the selectivity. As illustrated in Figure 3C, the FE<sub>CO</sub> of the NiPc cage exceeds 95% and exhibits only a slight fluctuation in the potential range from -0.8 to -1.3 V. The NiPc cage almost exclusively generates CO with a selectivity of 98.7% at -1.2 V, which is among the best catalytic performances for Pcbased molecular or polymeric materials. <sup>21–23,32–36</sup> However, the ZnPc cage exhibits a FE<sub>CO</sub> of less than 10% in the same potential range, again indicating that the NiPc cage has a superior catalytic activity over the ZnPc cage. These results show that tuning the metal center in Pcs is crucial to optimizing their activity and selectivity in the electrocatalytic CO<sub>2</sub>RR, which provides useful guidance for molecular catalysts in electrocatalysis. To investigate long-term stability, we conducted a 13 h chronoamperometric test at the potential of -1.2 V in CO<sub>2</sub>-saturated 0.1 M KHCO<sub>3</sub> solution and monitored the FE<sub>CO</sub> of the NiPc cage every hour during the entire experiment (Figure 3D). It was discovered that the  $FE_{CO}$  of the NiPc cage can be maintained at levels greater than 95% throughout the durability test, demonstrating its exceptional long-term stability (Figure S19).

Next, to demonstrate the advantage of molecular cages with isolated catalytic sites over aggregated small-molecule catalysts, we compared the CO<sub>2</sub>RR performance of the NiPc cage and NiPc-8OH under otherwise identical conditions (Figure 4A). Interestingly, even at an extremely negative potential of -2.0 V, the NiPc cage still retains a strong selectivity toward CO over  $H_2$  with a FE  $_{CO}$  of 93.5%. By contrast, the FE  $_{CO}$  for NiPc-8OH gradually enhances and reaches a maximum value of 87.2% at -1.2 V, then gradually decreases to 13.3% at -2 V. The TOFs of the NiPc cage and NiPc-8OH for CO production were also compared at the potential range from -0.8 to -1.3 V (Figure 4B). Notably, the TOF values of the NiPc cage are 56, 151, 249, 365, 506, and 606  $h^{-1}$  at -0.8, -0.9, -1, -1.1, -1.2, and -1.3 V, respectively, which are up to 13-fold larger than those of NiPc-8OH (6, 11, 22, 29, 40, and 45  $h^{-1}$ ). The higher CO<sub>2</sub>RR activity of the NiPc cage, compared with the small-molecule Pc derivative NiPc-8OH, is likely due to the increased exposure and accessibility of the catalytically active sites, which are spatially arranged in a rigid shape-persistent cage scaffold. <sup>22,23</sup> The porous cage structure could facilitate CO<sub>2</sub> diffusion and electrolyte penetration into multiple easily accessible catalytic metal centers, thus maximizing the usage of the electrocatalytic active sites (Table S2). 18,19 Moreover, the shape persistency of the cage structure precludes the aggregation of adjacent NiPc panels, which maintains the number of electrochemically accessible and active Pc centers.

In summary, we demonstrate the synthesis of shape-persistent Pc cages and their electrocatalytic activities in the  $\rm CO_2RR$ . The construction of the cages was accomplished through rational design and self-sorting of two different diol building blocks in the dynamic system, enabled by the reversible spiroborate formation. Two metallated Pc cages were successfully obtained, and the structure of one of the cages was

#### Report



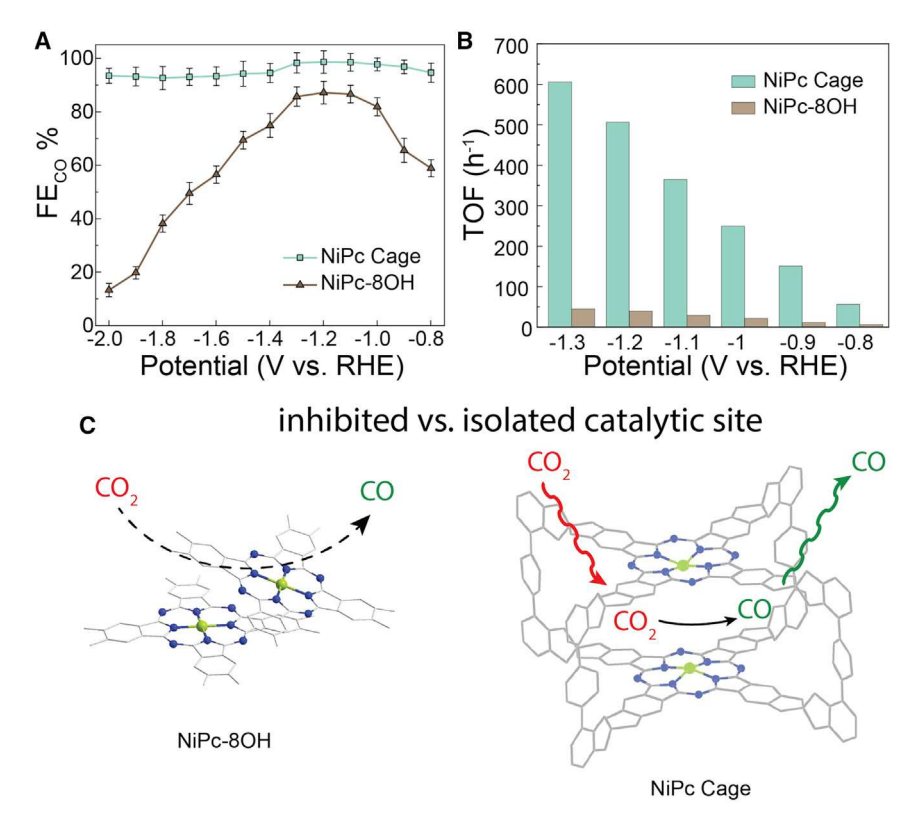


Figure 4. Catalytic performance comparison between NiPc cage and NiPc-8OH

- (A) CO faradaic efficiency of NiPc cage and NiPc-8OH.
- (B) TOF comparison of NiPc cage and NiPc-8OH.

(C) Partially blocked and readily accessible  $CO_2$  reduction catalytic center in aggerated NiPc-8OH monomer (left) and NiPc cage (right).

The error bars represent the standard deviation from at least three independent measurements.

resolved at the atomic level through single-crystal X-ray diffraction. The NiPc cage exhibits superior electrochemical performance for  ${\rm CO_2}$  reduction when compared with the ZnPc cage and the non-caged control molecules in this work, showing exceptional activity,  ${\rm CO/H_2}$  selectivity, and stability in a broad potential range. Even though these cages, as emerging electrocatalysts, still have limitations, such as their low electron conductivities, leading to relatively low current densities, it is anticipated that through further modification of their molecular structures to improve their intrinsic conductivities or integrating them into conductive frameworks, their electrocatalytic performance could be further enhanced. This study demonstrates the feasibility and significance of incorporating catalytically active moieties into well-defined molecular cage structures to achieve high catalytic performance and stability.

#### **EXPERIMENTAL PROCEDURES**

#### **Resource availability**

#### Lead contact

Further information and requests for resources and reagents should be directed to and will be fulfilled by the lead contact, Wei Zhang (wei.zhang@colorado.edu).

#### Materials availability

Details about the synthesis of materials and the data used to draw the conclusions can be found in the supplemental information.



#### Data and code availability

Details about the synthesis of materials and the data used to draw the conclusions can be found in the supplemental information. The accession number for the ZnPc cage reported in this paper is CCDC: 2160662.

#### **Methods and characterization**

See supplemental experimental procedures for full details of synthesis and characterization.

#### SUPPLEMENTAL INFORMATION

Supplemental information can be found online at https://doi.org/10.1016/j.xcrp. 2023.101285.

#### **ACKNOWLEDGMENTS**

W.Z. thanks the support from National Science Foundation (CHE-2108197). S.L. thanks the support from National Natural Science Foundation of China (52173201 and 21905115). NSF's ChemMatCARS Sector 15 is supported by the Divisions of Chemistry (CHE) and Materials Research (DMR), National Science Foundation, under grant number NSF/CHE-1834750. Use of the Advanced Photon Source, an Office of Science User Facility operated for the US Department of Energy (DOE) Office of Science by Argonne National Laboratory, was supported by the US DOE under contract no. DE-AC02-06CH11357. This research used the 17-ID-2 (FMX) beamline of the National Synchrotron Light Source II, a US DOE Office of Science User Facility operated for the DOE Office of Science by Brookhaven National Laboratory under contract no. DE-SC0012704.

#### **AUTHOR CONTRIBUTIONS**

Y.H. and W.Z. conceived the idea and designed the experiment. Y.H., L.J.W., J.W., Q.X., and H.C. performed the synthesis and analyzed the data. T.C., Y.-P.C., X.L., and B.A. carried out the single-crystal X-ray test. S.H., H.Z., M.D., and S.L. performed the electrochemical measurements. Y.H., S.H., Y.J., S.L., and W.Z. wrote the paper. All authors discussed the results and commented on the manuscript.

#### **DECLARATION OF INTERESTS**

The authors declare no competing interests.

Received: June 30, 2022 Revised: December 6, 2022 Accepted: January 19, 2023 Published: February 7, 2023

#### **REFERENCES**

- Tozawa, T., Jones, J.T.A., Swamy, S.I., Jiang, S., Adams, D.J., Shakespeare, S., Clowes, R., Bradshaw, D., Hasell, T., Chong, S.Y., et al. (2009). Porous organic cages. Nat. Mater. 8, 973–978.
- Mukhopadhyay, R.D., Kim, Y., Koo, J., and Kim, K. (2018). Porphyrin boxes. Acc. Chem. Res. 51, 2730–2738.
- Zhang, G., and Mastalerz, M. (2014).
   Organic cage compounds from shapepersistency to function. Chem. Soc. Rev. 43, 1934–1947.
- Jin, Y., Voss, B.A., Noble, R.D., and Zhang, W. (2010). A shape-persistent organic molecular cage with high selectivity for the adsorption of CO2 over N2. Angew. Chem., Int. Ed. Engl. 49, 6348-6351.
- Zhang, C., Wang, Q., Long, H., and Zhang, W. (2011). A highly C70 selective shape-persistent rectangular prism constructed through onestep alkyne metathesis. J. Am. Chem. Soc. 133, 20995–21001
- 6. Danjo, H., Masuda, Y., Kidena, Y., Kawahata, M., Ohara, K., and Yamaguchi, K. (2020).
- Preparation of cage-shaped hexakis(spiroborate)s. Org. Biomol. Chem. 18, 3717–3723.
- Lee, S., Yang, A., Moneypenny, T.P., and Moore, J.S. (2016). Kinetically trapped tetrahedral cages via alkyne metathesis. J. Am. Chem. Soc. 138, 2182–2185.
- Shi, Y., Cai, K., Xiao, H., Liu, Z., Zhou, J., Shen, D., Qiu, Y., Guo, Q.-H., Stern, C., Wasielewski, M.R., et al. (2018). Selective extraction of C70 by a tetragonal prismatic porphyrin cage. J. Am. Chem. Soc. 140, 13835–13842.

#### Report

OPEN ACCESS

- Liu, Y., Zhao, W., Chen, C.-H., and Flood Amar, H. (2019). Chloride capture using a C-H hydrogen-bonding cage. Science 365, 159–161.
- McCaffrey, R., Long, H., Jin, Y., Sanders, A., Park, W., and Zhang, W. (2014). Template synthesis of gold nanoparticles with an organic molecular cage. J. Am. Chem. Soc. 136, 1782–1785.
- Mondal, B., Acharyya, K., Howlader, P., and Mukherjee, P.S. (2016). Molecular cage impregnated palladium nanoparticles: efficient, additive-free heterogeneous catalysts for cyanation of aryl halides. J. Am. Chem. Soc. 138, 1709–1716.
- Qiu, L., McCaffrey, R., Jin, Y., Gong, Y., Hu, Y., Sun, H., Park, W., and Zhang, W. (2018). Cagetemplated synthesis of highly stable palladium nanoparticles and their catalytic activities in Suzuki–Miyaura coupling. Chem. Sci. 9, 676–680
- Sun, J.-K., Zhan, W.-W., Akita, T., and Xu, Q. (2015). Toward homogenization of heterogeneous metal nanoparticle catalysts with enhanced catalytic performance: soluble porous organic cage as a stabilizer and homogenizer. J. Am. Chem. Soc. 137, 7063–7066.
- Luo, N., Ao, Y.-F., Wang, D.-X., and Wang, Q.-Q. (2021). Exploiting anion-π interactions for efficient and selective catalysis with chiral molecular cages. Angew. Chem., Int. Ed. Engl. 60, 20650–20655.
- Koo, J., Kim, I., Kim, Y., Cho, D., Hwang, I.-C., Mukhopadhyay, R.D., Song, H., Ko, Y.H., Dhamija, A., Lee, H., et al. (2020). Gigantic porphyrinic cages. Chem 6, 3374–3384.
- Takezawa, H., Shitozawa, K., and Fujita, M. (2020). Enhanced reactivity of twisted amides inside a molecular cage. Nat. Chem. 12, 574–578.
- Hong, S., Rohman, M.R., Jia, J., Kim, Y., Moon, D., Kim, Y., Ko, Y.H., Lee, E., and Kim, K. (2015). Porphyrin boxes: rationally designed porous organic cages. Angew. Chem., Int. Ed. Engl. 54, 13241–13244.
- Smith, P.T., Benke, B.P., Cao, Z., Kim, Y., Nichols, E.M., Kim, K., and Chang, C.J. (2018). Iron porphyrins embedded into a supramolecular porous organic cage for electrochemical CO2 reduction in water. Angew. Chem., Int. Ed. Engl. 57, 9684–9688.
- 19. Smith, P.T., Kim, Y., Benke, B.P., Kim, K., and Chang, C.J. (2020). Supramolecular tuning

- enables selective oxygen reduction catalyzed by cobalt porphyrins for direct electrosynthesis of hydrogen peroxide. Angew. Chem., Int. Ed. Engl. 59, 4902–4907.
- Benke, B.P., Aich, P., Kim, Y., Kim, K.L., Rohman, M.R., Hong, S., Hwang, I.-C., Lee, E.H., Roh, J.H., and Kim, K. (2017). lodide-Selective synthetic ion channels based on shape-persistent organic cages. J. Am. Chem. Soc. 139, 7432–7435.
- Han, B., Ding, X., Yu, B., Wu, H., Zhou, W., Liu, W., Wei, C., Chen, B., Qi, D., Wang, H., et al. (2021). Two-dimensional covalent organic frameworks with cobalt(II)-Phthalocyanine sites for efficient electrocatalytic carbon dioxide reduction. J. Am. Chem. Soc. 143, 7104–7113.
- Han, B., Jin, Y., Chen, B., Zhou, W., Yu, B., Wei, C., Wang, H., Wang, K., Chen, Y., Chen, B., and Jiang, J. (2022). Maximizing electroactive sites in a three-dimensional covalent organic framework for significantly improved carbon dioxide reduction electrocatalysis. Angew. Chem., Int. Ed. Engl. 61, e202114244.
- Zhang, M.-D., Si, D.-H., Yi, J.-D., Zhao, S.-S., Huang, Y.-B., and Cao, R. (2020). Conductive phthalocyanine-based covalent organic framework for highly efficient electroreduction of carbon dioxide. Small 16, 2005254.
- Wang, N., Yao, K., Vomiero, A., Wang, Y., and Liang, H. (2021). Inhibiting carbonate formation using CO2–CO–C2+ tandems. SmartMat 2, 423–425.
- Reddu, V., Sun, L., Li, X., Jin, H., Wang, S., and Wang, X. (2022). Highly selective and efficient electroreduction of CO2 in water by quaterpyridine derivative-based molecular catalyst noncovalently tethered to carbon nanotubes. SmartMat 3, 151–162.
- Yang, C., Gao, Z., Wang, D., Li, S., Li, J., Zhu, Y., Wang, H., Yang, W., Gao, X.J., Zhang, Z., and Hu, W. (2022). Bimetallic phthalocyanine heterostructure used for highly selective electrocatalytic CO2 reduction. Sci. China Mater. 65, 155–162.
- 27. Gouloumis, A., González-Rodríguez, D., Vázquez, P., Torres, T., Liu, S., Echegoyen, L., Ramey, J., Hug, G.L., and Guldi, D.M. (2006). Control over charge separation in Phthalocyanine—Anthraquinone conjugates as a function of the aggregation status. J. Am. Chem. Soc. 128, 12674–12684.
- Tolbin, A.Y., Ivanov, A.V., Tomilova, L.G., and Zefirov, N.S. (2003). Synthesis of 1,2-bis(3,4dicyanophenoxymethyl)benzene and binuclear

- zinc phthalocyanines of clamshell and ball types. J. Porphyr. Phthalocyanines 07, 162–166.
- Hu, Y., Teat, S.J., Gong, W., Zhou, Z., Jin, Y., Chen, H., Wu, J., Cui, Y., Jiang, T., Cheng, X., and Zhang, W. (2021). Single crystals of mechanically entwined helical covalent polymers. Nat. Chem. 13, 660–665.
- Wang, X., Bahri, M., Fu, Z., Little, M.A., Liu, L., Niu, H., Browning, N.D., Chong, S.Y., Chen, L., Ward, J.W., and Cooper, A.I. (2021). A cubic 3D covalent organic framework with nbo topology. J. Am. Chem. Soc. 143, 15011– 15016.
- Hu, Y., Dunlap, N., Long, H., Chen, H., Wayment, L.J., Ortiz, M., Jin, Y., Nijamudheen, A., Mendoza-Cortes, J.L., Lee, S.-h., and Zhang, W. (2021). Helical covalent polymers with unidirectional ion channels as single lithium-ion conducting electrolytes. CCS Chem. 3, 2762–2770.
- Huang, N., Lee, K.H., Yue, Y., Xu, X., Irle, S., Jiang, Q., and Jiang, D. (2020). A stable and conductive metallophthalocyanine framework for electrocatalytic carbon dioxide reduction in water. Angew. Chem., Int. Ed. Engl. 59, 16587– 16593.
- 33. Lu, M., Zhang, M., Liu, C.-G., Liu, J., Shang, L.-J., Wang, M., Chang, J.-N., Li, S.-L., and Lan, Y.-Q. (2021). Stable dioxinlinked metallophthalocyanine covalent organic frameworks (COfs) as photocoupled electrocatalysts for CO2 reduction. Angew. Chem., Int. Ed. Engl. 60, 4864–4871.
- 34. Yi, J.-D., Si, D.-H., Xie, R., Yin, Q., Zhang, M.-D., Wu, Q., Chai, G.-L., Huang, Y.-B., and Cao, R. (2021). Conductive two-dimensional phthalocyanine-based metal-organic framework nanosheets for efficient electroreduction of CO2. Angew. Chem., Int. Ed. Engl. 60, 17108–17114.
- Meng, Z., Luo, J., Li, W., and Mirica, K.A. (2020). Hierarchical tuning of the performance of electrochemical carbon dioxide reduction using conductive two-dimensional metallophthalocyanine based metal–organic frameworks. J. Am. Chem. Soc. 142, 21656– 21669.
- Yue, Y., Cai, P., Xu, K., Li, H., Chen, H., Zhou, H.-C., and Huang, N. (2021). Stable bimetallic polyphthalocyanine covalent organic frameworks as superior electrocatalysts. J. Am. Chem. Soc. 143, 18052–18060.